Two-Dimensional Semiconductor Device Simulation of Trap-Assisted Generation-Recombination Noise Under Periodic Large-Signal Conditions and Its Use for Developing Cyclostationary Circuit Simulation Models

Juan E. Sanchez, *Member, IEEE*, Gijs Bosman, *Senior Member, IEEE*, and Mark E. Law, *Fellow, IEEE*

***Abstract*—The simulation of generation-recombination (GR) noise under periodic large-signal conditions in a partial differential equation-based silicon device simulator is presented. Using the impedance-field method with cyclostationary noise sources, it is possible to simulate the self- and cross-spectral densities between sidebands of a periodic large-signal stimulus. Such information is needed to develop noise correlation matrices for use with a circuit simulator. Examples are provided which demonstrate known results for shot noise in bipolar junction transistors. Additional results demonstrate the upconversion of low-frequency GR noise for microscopically cyclostationary noise sources and provide evidence for applying the modulated stationary noise model for low-frequency noise when there is a nearly quadratic current dependence.**

***Index Terms*—Correlation, frequency conversion, mixer noise, nonlinear circuits, nonlinear systems, semiconductor device modeling, semiconductor device noise.**

I. Introduction

THE FREQUENCY conversion of noise under periodic large-signal conditions is of active interest to both the device physics and circuit design communities [1], [2]. It has a significant effect on the performance of wireless communications circuits, such as the spectral purity of oscillators and the noise figure of mixers.

While the conversion of shot and thermal noise is well understood and has successfully been modeled for circuit simulation using noise correlation matrices (NCMs) [3], [4], the modulation of $1/f$-like low-frequency noise is still an open topic [5], [6]. This is, in part, due to the fact that such low-frequency noise can be attributed to a variety of sources [7]. In addition, the contribution of such noise sources is dependent on its spatial location and the unknown time-varying bias dependence of their autocorrelation.

Manuscript received November 4, 2002; revised January 22, 2003. This work was supported by the Semiconductor Research Corporation (SRC). The review of this paper was arranged by Editor J. Deen.

J. E. Sanchez was with the Department of Electrical and Computer Engineering, University of Florida, Gainesville, FL 32611 USA. He is now with Synopsys, Inc., Mountain View, CA 94043 USA (e-mail: j.sanchez@ieee.org).

G. Bosman and M. E. Law are with the Department of Electrical and Computer Engineering, University of Florida, Gainesville, FL 32611 USA.

Digital Object Identifier 10.1109/TED.2003.813448

The impedance field method (IFM) originally referred to the coupling of current-density (velocity) fluctuations within the semiconductor to an open-circuit voltage at the contacts of the device [8]. This method was typically used to get analytic results for both velocity fluctuation and generation-recombination (GR) transition-rate fluctuations [9]. The IFM was extended to partial differential equation (PDE)-based semiconductor device simulation [10]. These techniques were then extrapolated for the case of device simulation of cyclostationary noise under periodic steady-state conditions [1], [11]. In [12], the authors present simulation results for microscopically cyclostationary trap-assisted GR noise sources.

The drift-diffusion simulation of semiconductor devices requires the solution of the Poisson, electron-continuity, and hole-continuity equations for each differential volume within a semiconductor mesh. In order to consider an indirect recombination or trapping process which results in frequency-dependent noise, it is also necessary to consider a trap-continuity equation. The Florida object-oriented device simulator (FLOODS) [13], [14] has been enhanced with noise simulation capability for one-dimensional (1-D) and two-dimensional (2-D) semiconductor devices under both dc and periodic time-varying bias conditions. This tool is capable of solving for an arbitrary number of user-defined PDEs. In addition, the auto- and cross correlation of the Langevin terms of the IFM are specified for each PDE. As a research tool, this software is being used to investigate both GR and diffusion noise and the resulting effect on the device performance in silicon.

In Section II, we review the IFM generalized to periodic large-signal conditions. The modulated stationary noise model is applied for the case of trap-assisted GR noise. Section III presents the NCM, which is used in circuit simulation to model cyclostationary equivalent current noise sources. We discuss how the NCM can be extracted through semiconductor device simulation. We then develop the NCM model for the case of microscopically stationary GR noise for comparison with simulation results.

In Section IV, simulation results are presented for the frequency conversion of both diffusion noise and trap-assisted GR noise under periodic large-signal conditions for a bipolar junction transistor (BJT). While the focus of this paper is on GR

0018-9383/03$17.00 © 2003 IEEE

noise, diffusion noise simulations are included to observe the relative importance and frequency conversion characteristics of the two noise components. We also simulate the cross-spectral densities (CSDs) between sidebands for both the case of diffusion noise and trap-assisted GR noise. Well-known results for the NCM for shot noise [3], [4] in junctions are verified using the simulator. In addition, we present simulation results which show good agreement between the modulated stationary noise model [15], [5], [6] for low-frequency noise in circuit simulation and microscopically cyclostationary GR noise sources in semiconductor device simulation.

II. Noise Simulation Under Periodic Large-Signal Conditions

A. Periodic Steady State

When a periodic bias with a fundamental frequency of ω is applied to a semiconductor device terminal, the nonlinear relationship between ψ, n, p, and n_t (see Table I) results in frequency components of these quantities being generated at integer multiples of ω. For example, the time-varying potential is then

$$\psi(t, r) = \sum_{k=-\infty}^{\infty} \Psi(\omega_k, r) e^{j\omega_k t} \tag{1}$$

where $\Psi(\omega_k, r)$ is the kth harmonic of the potential at position r in the device and ω_k is the harmonic frequency (see Table II).

The harmonic balance (HB) method is used to find the periodic steady-state solution of the semiconductor device. This is a frequency-domain technique in which the Fourier coefficients of the solution variables are found [16]. Since it is necessary to solve for all frequency components for each equation at each node in the semiconductor mesh simultaneously, the resulting matrix is often too large to solve using direct methods. Recent advances in the use of iterative methods for HB circuit simulation have been applied to semiconductor simulation so that it is a tractable problem for modern computer workstations [17].

While time-domain methods such as the transient or shooting method could be used to find the periodic steady state [18], the advantage of the HB method is that the procedure to find the linearized equations used to converge upon a solution can also be used for finding the small-signal conversion matrix required for a noise analysis.

B. Impedance Field Method

By linearizing the frequency-domain equations, a linear periodically time-varying (LPTV) system is formed which models how fluctuations within the semiconductor are frequency converted between sidebands of the large-signal currents flowing through the device. As depicted in Fig. 1, we consider harmonically related phasors for each sideband $\tilde{\omega}_k$, where $k < 0$ for a lower sideband (LSB), $k = 0$ for the baseband (BB), and $k > 0$ for an upper sideband (USB). Being real signals, each of these phasors has a complex conjugate at $\omega_k - \tilde{\omega}_0$.

We use the Shockley–Read–Hall (SRH) recombination model [19], which is depicted in Fig. 2, to describe band transitions and noise. Table I defines the parameters used in the SRH equations. For one trap level, the trap-continuity equation is then

$$\frac{\partial n_t}{\partial t} = R_n - G_n - R_p + G_p + \tilde{\gamma}_{n_t} \tag{2}$$

and the electron- and hole-continuity equations are

$$\frac{\partial n}{\partial t} = \frac{1}{q} \nabla \cdot J_n + G_n - R_n + \tilde{\gamma}_n \tag{3}$$

TABLE I
Device Simulation Variables

ψ	Potential	$/\mathrm{cm}^3$
n	Electron carrier density	$/\mathrm{cm}^3$
p	Hole carrier density	$/\mathrm{cm}^3$
n_i	Intrinsic carrier density, $n_i = n_1 p_1$	$/\mathrm{cm}^3$
n_1	n when quasi-Fermi level crosses trap	$/\mathrm{cm}^3$
p_1	p when quasi-Fermi level crosses trap	$/\mathrm{cm}^3$
n_t	Trapped electron density	$/\mathrm{cm}^3$
N_t	Trap density	$/\mathrm{cm}^3$
N_t^D	Neutral Donor Trap density	$/\mathrm{cm}^3$
c_n	Capture coefficient for electrons, $e_n n_1$	$\mathrm{cm}^3/\mathrm{sec}$
c_p	Capture coefficient for holes, $e_p p_1$	$\mathrm{cm}^3/\mathrm{sec}$
e_n, e_p	Emission coefficient for electrons, holes	$\mathrm{cm}^6/\mathrm{sec}$
G_n	Electron generation rate, $e_n n_t$	$1/\mathrm{cm}^3\mathrm{sec}$
R_n	Electron recombination rate, $c_n n (N_t - n_t)$	$1/\mathrm{cm}^3\mathrm{sec}$
G_p	Hole recombination rate, $c_p p n_t$	$1/\mathrm{cm}^3\mathrm{sec}$
R_p	Hole generation rate, $e_p (N_t - n_t)$	$1/\mathrm{cm}^3\mathrm{sec}$

TABLE II
Frequency Domain Quantities

t	Time	sec
ω	Fundamental frequency of periodic large-signal	rad/sec
ω_k	Harmonic at $k\omega$	rad/sec
$\tilde{\omega}_0$	Baseband small-signal frequency	rad/sec
$\tilde{\omega}_k$	Sideband at $\omega_k + \tilde{\omega}_0$	rad/sec
$\tilde{\varphi}_k$	Phase angle of phasor at $\tilde{\omega}_k$	rad

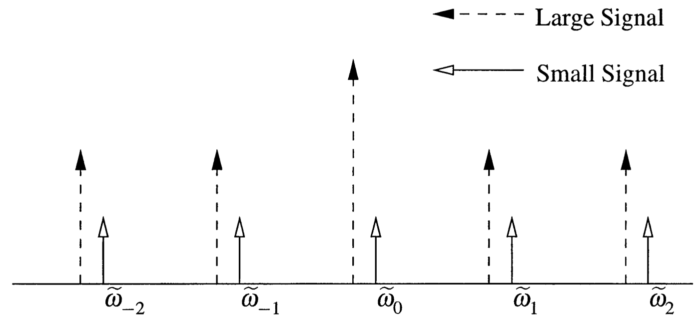

Fig. 1. Small-signal noise representation.

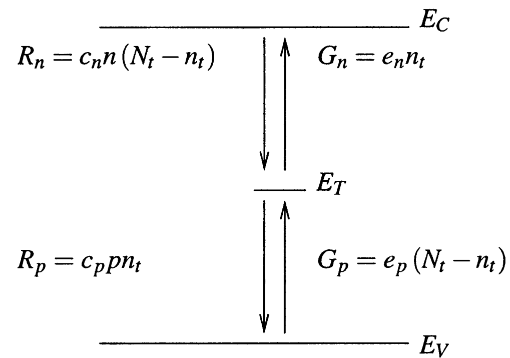

Fig. 2. SRH GR process. Arrows show electron transitions.

$$\frac{\partial p}{\partial t} = -\frac{1}{q}\nabla \cdot J_p + G_p - R_p + \tilde{\gamma}_p \tag{4}$$

and Poisson's equation is stated as

$$\nabla^2 \psi = -\frac{q}{\varepsilon}\left(p - n + N_D - N_A + N_t^D - n_t\right) \tag{5}$$

where N_t^D is the density of donor-like traps, and $\tilde{\gamma}_n$, $\tilde{\gamma}_p$, and $\tilde{\gamma}_{n_t}$ are the Langevin terms corresponding to fluctuations in the steady-state GR transition rates in the electron-, hole-, and trap-continuity equations, respectively.

By placing a source $\tilde{\gamma}_\alpha$ in each linearized PDE describing the semiconductor device, it is possible to couple perturbations in the microscopic GR rates in the semiconductor with a voltage or current response at the device terminals. For trap-assisted GR fluctuations, the cross-spectral density between a response at external circuit node x at $\tilde{\omega}_k$ and node y at $\tilde{\omega}_l$ is

$$S_{gr}^{x,y}(\tilde{\omega}_k, \tilde{\omega}_l) = \int_r \sum_{\alpha,\beta=n,p,n_t} \sum_{u,v=-\infty}^{\infty} \tilde{G}_\alpha^x(\tilde{\omega}_k, \tilde{\omega}_u, r) \times K_{\tilde{\gamma}_\alpha,\tilde{\gamma}_\beta}(\tilde{\omega}_u, \tilde{\omega}_v, r) \cdot \tilde{G}_\beta^y(\tilde{\omega}_l, \tilde{\omega}_v, r)^* \partial r \tag{6}$$

where $\tilde{G}_\alpha^x(\tilde{\omega}_k, \tilde{\omega}_u, r)$ is the scalar Green's function which couples GR fluctuations for each differential volume r from the electron- ($\alpha = n$), hole- ($\alpha = p$), or trap- ($\alpha = n_t$) continuity equation at frequency $\tilde{\omega}_u$ to a response at circuit node x at frequency $\tilde{\omega}_k$. Using modified nodal analysis, x and y can also represent current through a voltage source [20]. The noise source strength $K_{\tilde{\gamma}_\alpha,\tilde{\gamma}_\beta}(\tilde{\omega}_u, \tilde{\omega}_v, r)$ accounts for the correlation of transition-rate fluctuations between equations α and β at sideband frequencies $\tilde{\omega}_u$ and $\tilde{\omega}_v$, respectively, and is defined in the next section.

Diffusion noise is found using [1], [11]

$$S_{\text{diff}}^{x,y}(\tilde{\omega}_k, \tilde{\omega}_l) = \int_r \sum_{\alpha=n,p} \sum_{u,v=-\infty}^{\infty} \vec{G}_\alpha^x(\tilde{\omega}_k, \tilde{\omega}_u, r) \times K_{\vec{\xi}_\alpha,\vec{\xi}_\alpha}(\tilde{\omega}_u, \tilde{\omega}_v, r) \cdot \vec{G}_\alpha^y(\tilde{\omega}_l, \tilde{\omega}_v, r)^* \partial r \tag{7}$$

where

$$\vec{G}_\alpha^x(\tilde{\omega}_k, \tilde{\omega}_u, r) = \frac{1}{q}\nabla \tilde{G}_\alpha^x(\tilde{\omega}_k, \tilde{\omega}_u, r) \tag{8}$$

is the vector Green's function and $K_{\vec{\xi}_\alpha,\vec{\xi}_\alpha}(\tilde{\omega}_u, \tilde{\omega}_v, r)$ is the noise source strength tensor for velocity fluctuations.

The total CSD is then given by

$$S_{\text{total}}^{x,y}(\tilde{\omega}_k, \tilde{\omega}_l) = S_{gr}^{x,y}(\tilde{\omega}_k, \tilde{\omega}_l) + S_{\text{diff}}^{x,y}(\tilde{\omega}_k, \tilde{\omega}_l). \tag{9}$$

C. Cyclostationary Noise Analysis

1) Modulated Stationary Noise Model: We use the modulated stationary noise model [6] to model the instantaneous bias dependence of the microscopic noise sources. This model has been used to describe the modulation of shot noise in diodes [3], [4] in circuit simulation and has been recently applied to the modulation of microscopic noise sources in device simulation [11]. This model applies when the correlation time of a noise process is much shorter than the period of an applied large-signal bias and is applicable to microscopic diffusion noise and GR noise phenomena. Consider a noise process given by

$$n(t) = \sqrt{f(t)}x(t) \tag{10}$$

where $f(t)$ is the modulating function described by

$$f(t) = \sum_{k=-\infty}^{\infty} F(\omega_k)e^{j\omega_k t} \tag{11}$$

and is an instantaneous function of the solution variables and $x(t)$ is a unit stationary noise source with

$$x(t) = \sum_{k=-\infty}^{\infty} e^{j\tilde{\omega}_k t} e^{j\tilde{\varphi}_k} \tag{12}$$

where $\tilde{\varphi}_k$ is a random phase angle and $R_{x,x}(t, t+\tau) = \delta(\tau)$.

It can be shown that the CSD between noise phasors at sideband frequencies $\tilde{\omega}_k$ and $\tilde{\omega}_l$ is then [3]

$$S_n(\tilde{\omega}_k, \tilde{\omega}_l) = F(\omega_{k-l}). \tag{13}$$

In order to properly account for the total noise, it is necessary to account for the contribution of both the self- and cross-spectral components to the output response of the semiconductor device through the time-varying Green's functions as described by (6) and (7).

2) GR Noise Sources: If the fundamental source of the $1/f$-like fluctuations in a semiconductor can be attributed to GR events, it is possible to apply the IFM and the modulated stationary noise model so that low-frequency noise can be simulated under periodic large-signal conditions. The GR transition-rate fluctuations between the conduction or valence band and the trap level are white processes so that (13) applies. For one trap level, the time-derivative term in (2) often results in a Lorentzian frequency spectrum when coupled to the device contact. For a proper distribution in energy or position for the traps, the low-frequency noise can produce a $1/f$ spectrum [21].

Being a shot process, the microscopic GR noise sources have an autocorrelation of [9]

$$R_{\tilde{\gamma}_\alpha,\tilde{\gamma}_\alpha}(t, t+\tau) = 2(G_\alpha(t) + R_\alpha(t))\delta(\tau) \tag{14}$$

and $G_\alpha(t)$ and $R_\alpha(t)$ are the instantaneous GR rates between the conduction band ($\alpha = n$) or valence band ($\alpha = p$) and the trap level. Using (13), the noise source strengths for use in (6) are then

$$K_{\tilde{\gamma}_n,\tilde{\gamma}_n}(\tilde{\omega}_u, \tilde{\omega}_v, r) = -K_{\tilde{\gamma}_{n_t},\tilde{\gamma}_n}(\tilde{\omega}_u, \tilde{\omega}_v, r) = S_{\tilde{\gamma}_n}(\omega_{u-v}, r) \tag{15}$$

$$K_{\tilde{\gamma}_p,\tilde{\gamma}_p}(\tilde{\omega}_u, \tilde{\omega}_v, r) = K_{\tilde{\gamma}_p,\tilde{\gamma}_{n_t}}(\tilde{\omega}_u, \tilde{\omega}_v, r) = S_{\tilde{\gamma}_p}(\omega_{u-v}, r) \tag{16}$$

$$K_{\tilde{\gamma}_{n_t},\tilde{\gamma}_{n_t}}(\tilde{\omega}_u, \tilde{\omega}_v, r) = K_{\tilde{\gamma}_n,\tilde{\gamma}_n}(\tilde{\omega}_u, \tilde{\omega}_v, r) + K_{\tilde{\gamma}_p,\tilde{\gamma}_p}(\tilde{\omega}_u, \tilde{\omega}_v, r) \tag{17}$$

$$K_{\tilde{\gamma}_n,\tilde{\gamma}_p}(\tilde{\omega}_u, \tilde{\omega}_v, r) = K_{\tilde{\gamma}_p,\tilde{\gamma}_n}(\tilde{\omega}_u, \tilde{\omega}_v, r) = 0 \tag{18}$$

where

$$S_{\tilde{\gamma}_\alpha}(\omega_k, r) = 2G_\alpha(\omega_k, r) + 2R_\alpha(\omega_k, r) \tag{19}$$

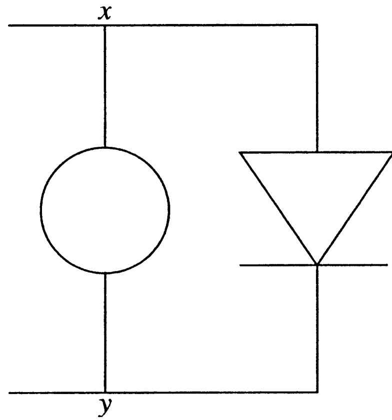

Fig. 3. Equivalent noise current generator.

where $G_\alpha(\omega_k, r)$ and $R_\alpha(\omega_k, r)$ are the Fourier coefficients of the spatially dependent generation and recombination rates, respectively.

3) Diffusion Noise Sources: The noise source strength tensor used in (7) for velocity fluctuations is

$$K_{\vec{\xi}_\alpha, \vec{\xi}_\alpha}(\tilde{\omega}_u, \tilde{\omega}_v, r) = 4q^2 D_\alpha \alpha(\omega_{u-v}, r) \tag{20}$$

where D_α is the diffusivity and $\alpha(\omega_k, r)$ is the kth harmonic of the carrier density. For the purposes of our investigation, we use the Einstein relationship

$$D_\alpha = \frac{kT\mu_\alpha}{q} \tag{21}$$

to find the noise source from the low-field mobility. For 2-D and three-dimensional (3-D) simulation it is appropriate to use a frequency dependent diffusivity tensor to account for crystallographic direction [1] and frequency components of the diffusivity/carrier-density product to account for the electric field dependence of the diffusivity [11]. Since our focus is the $1/f$-like low-frequency noise, no attempt was made to account for the diffusivity outside of equilibrium. This microscopic noise source results in shot noise observed in diodes and thermal noise in resistors. An additional reduced shot noise component may stem from GR transitions in the quasi-neutral regions and is accounted for by (14)–(19) [9].

III. NCM FOR CIRCUIT SIMULATION

A. Theory

For dc steady-state noise analysis in circuits, an equivalent current-noise generator is used to model the noise of the semiconductor devices in a circuit at the small-signal frequency being considered. The current generator for a two-terminal junction device is shown in Fig. 3. While our simulation results in Section IV are for a three-terminal device, we limit our discussion to this device in order to simplify the multiport frequency discussion.

Since the noise is instantaneously dependent on bias, an NCM is required to account for the cross correlation between the current phasors at each sideband under periodic large-signal conditions. If the large-signal behavior of an equivalent noise generator for circuit simulation is unknown, we show in this section how it may be found by modeling the fundamental noise sources in a semiconductor device simulator.

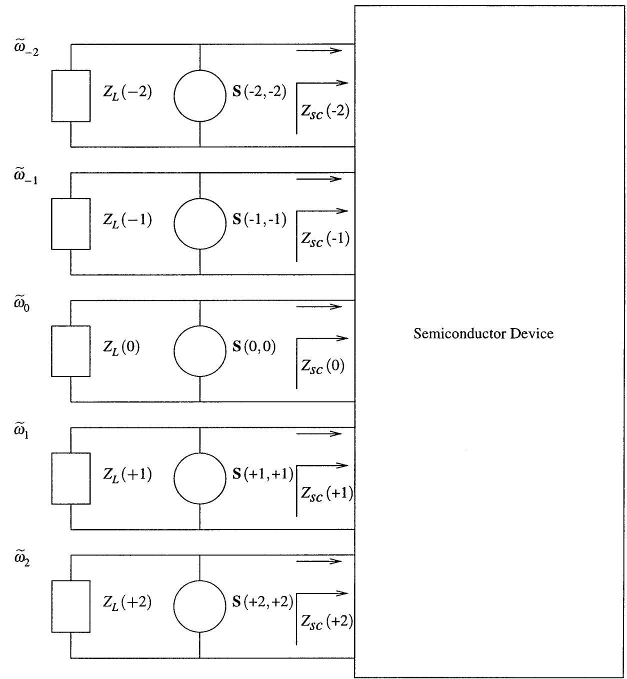

Fig. 4. Network representation of correlated noise generators for a one-port device.

When a device is placed in a circuit under periodic steady-state conditions, the response is

$$\delta\mathbf{V} = \mathbf{Y}^{-1}\delta\mathbf{I} \tag{22}$$

where $\delta\mathbf{I}$ is a vector of correlated current phasors at the harmonically related sideband frequencies, $\mathbf{Y}$ is the admittance matrix formed by linearizing the nodal circuit equations, and $\delta\mathbf{V}$ is the voltage response at each sideband for every node in the circuit [22]. Using modified nodal analysis [20], the current response through each voltage source is also found.

The resulting noise spectral density at node i and frequency $\tilde{\omega}_k$ is then

$$S_{v_i, v_i}(\tilde{\omega}_k, \tilde{\omega}_k) = \mathbf{Z}_{i,k}\mathbf{S}\mathbf{Z}_{i,k}^\dagger \tag{23}$$

where $\mathbf{Z}_{i,k}$ is the row of $\mathbf{Y}^{-1}$ corresponding to output node i at frequency $\tilde{\omega}_k$, $\dagger$ denotes the transpose conjugate, and $\mathbf{S} = \langle \delta\mathbf{I} \;\; \delta\mathbf{I}^\dagger \rangle$ is the NCM where each column is a vector of correlated noise components.

Fig. 4 shows a network representation of how noise current generators at each sideband frequency contribute to the total noise spectral density for a one-port device. A port representing sideband $\tilde{\omega}_k$ has a noise generator $\mathbf{S}(k, k)$, which represents the current spectral density at that sideband. The input impedance of the semiconductor device at $\tilde{\omega}_k$ is represented by $Z_{sc}(k)$. In addition, $Z_L(k)$ represents the impedance of the termination presented to the device. A large-signal voltage source applied directly to the device presents a short-circuit condition to each sideband frequency, $\tilde{\omega}_k$, so that the noise generator at each frequency is unable to mix to other sidebands via the impedance of the device. A noise simulation under this condition would also

result in $S_{v_i, v_i}(\tilde{\omega}_k, \tilde{\omega}_k) = \mathbf{S}(k, k)$. In addition, a cross-spectral density simulation between sidebands k and l would result in $S_{v_i, v_i}(\tilde{\omega}_k, \tilde{\omega}_l) = \mathbf{S}(k, l)$.

Using a semiconductor device simulator, (6) can be used to find the NCM entries for low-frequency GR noise sources for use in circuit simulation. If an equivalent current noise generator has been placed between nodes x and y in a compact noise model, its NCM for low-frequency GR noise can be simulated in a semiconductor device simulator by placing a large-signal voltage source between these same nodes. The resulting NCM entry relating a current generator connected between nodes x and y at sideband frequencies $\tilde{\omega}_k$ and $\tilde{\omega}_l$ is then

$$\mathbf{S}_{x,y}(k, l) = S_{gr}^{x,y}(\tilde{\omega}_k, \tilde{\omega}_l). \tag{24}$$

In Section IV, simulation results are presented which demonstrate how this method is used to generate the NCM entries for low-frequency cyclostationary trap-assisted GR noise sources. The methodology presented in this section is adequate for simulation of an intrinsic device. In the case of an extrinsic resistance, the model in Fig. 3 would require the addition of a series element between the intrinsic device and the device terminal [23]. This method could then only be used if these parasitics are small enough as to not interfere with the large-signal operation of the device. In addition, the resistance must then be much smaller than the small-signal input impedance of the intrinsic device throughout the entire range of the applied bias.

While it is not always possible to generate an analytical model from such information, we attempt to apply known compact cyclostationary noise models for shot noise in diodes [3] and microscopically stationary low-frequency noise in linear resistors [23]–[25] to a BJT.

B. Diffusion Noise

For a junction diode, the shot noise is instantaneously dependent on bias so that the current spectral density observed at all small-signal frequencies is

$$S_i(t) = 2qi(t) \tag{25}$$

where $i(t)$ is the large-signal current and $S_i(t)$ has units of A^2/Hz. Using (13), the NCM entries which couple the noise generator at $\tilde{\omega}_k$ with the noise generator at $\tilde{\omega}_l$ are [4]

$$\mathbf{S}_{x,x}(k, l) = \mathbf{S}_{y,y}(k, l) = 2qI(\omega_{k-l}) \tag{26}$$

$$\mathbf{S}_{x,y}(k, l) = \mathbf{S}_{y,x}^*(k, l) = -2qI(\omega_{k-l}) \tag{27}$$

where $I(\omega_{k-l})$ is the $(k-l)$th harmonic of the large-signal current flowing through the diode and x and y are the nodes to which the current generator is attached (see Fig. 3). The minus sign in (27) accounts for the fact that current phasors entering node x are leaving node y.

C. GR Noise

The GR transition rates may be invariant (stationary) or variant (cyclostationary) with respect to an applied periodic bias. Regardless of whether or not the microscopic noise sources are bias dependent, a compact model would require an NCM. This is since harmonics of the periodic scalar Green's functions could modulate bias independent GR fluctuations into correlated current density fluctuations at the device terminals.

In the literature, $1/f$-like noise and GR noise have been observed in resistors and junction devices, such as bipolar junction transistors [26]. For GR noise the spectra is often observed as

$$S_i(\tilde{\omega}) = \frac{CI^\beta}{1 + \tilde{\omega}^2\tau^2} \tag{28}$$

where I is the dc current flowing into the device and $\beta \approx 2$. The equivalent noise generator for low-frequency noise in a BJT model is often placed between the base and emitter junction [26] and dependent on the base current. It is not known how these noise sources vary under large-signal bias conditions when the microscopic noise sources in the internal device are bias dependent.

For a resistor, low-frequency GR fluctuations may be viewed as bias independent (stationary) resistivity fluctuations which are modulated by the large-signal currents flowing through the device so that correlated current components exist at each sideband [12]. The current spectral density is then quadratically dependent on the current flowing through the device. In this section, we develop this model and in Section IV we investigate if this model can be more generally applied to noise in a BJT device.

If we consider these resistivity fluctuations as being stationary, the modulated stationary model applies, except that the stationary noise source is lowpass filtered. Equation (12) becomes

$$x(t) = \sum_{k=-\infty}^{\infty} \alpha(\tilde{\omega}_k) e^{j\tilde{\omega}_k t} e^{j\tilde{\varphi}_k} \tag{29}$$

where $\alpha(\tilde{\omega}_k)$ is function of frequency. The CSD between sidebands is then

$$S_n(\tilde{\omega}_k, \tilde{\omega}_l) = \sum_{u=-\infty}^{\infty} H(\omega_{k-u}) |\alpha(\tilde{\omega}_u)|^2 H^*(\omega_{l-u}) \tag{30}$$

where

$$H(\omega_u) = \frac{\omega_1}{2\pi} \int_0^{2\pi/\omega_1} \sqrt{f(t)} e^{-j\omega_u t}. \tag{31}$$

The NCM entries for a stationary low-frequency noise source with a quadratic current-dependence are then

$$\begin{aligned}\mathbf{S}_{x,x}(k, l) &= \mathbf{S}_{y,y}(k, l) = -\mathbf{S}_{x,y}(k, l) \\ &= \sum_{u=-\infty}^{\infty} I(\omega_{k-u}) c(\tilde{\omega}_u) I(\omega_{l-u})^*\end{aligned} \tag{32}$$

where $c(\tilde{\omega}_u) = |\alpha(\tilde{\omega}_u)|^2$. For a single trap

$$c(\tilde{\omega}_u) = \frac{C}{1 + \tilde{\omega}_u^2 \tau^2} \tag{33}$$

where C and τ are constants. For flicker noise

$$c(\tilde{\omega}_u) = \frac{C}{\tilde{\omega}_u}. \tag{34}$$

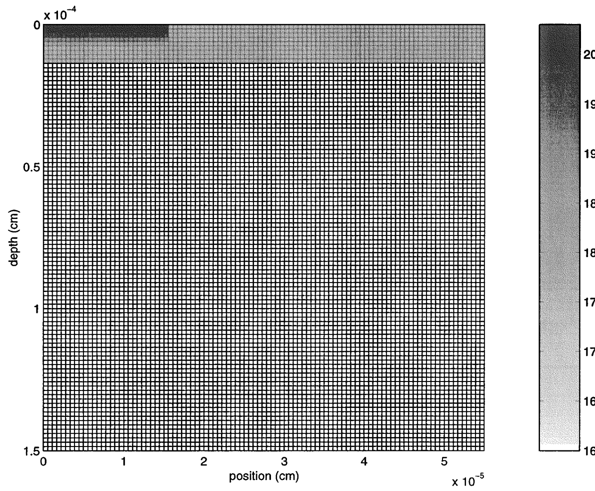

Fig. 5. BJT doping profile. Greyscale units are $\log_{10}|N_D - N_A|$. 0.15-μm emitter contact is located at the upper-left corner, the collector contact is along the bottom, and the 0.15-μm base contact is located at the upper-right-hand side.

For RF and microwave applications, $c(\tilde{\omega}_k) \approx 0$ for $|k| > 0$ and $\omega_1 \gg \tilde{\omega}_0$ so that

$$\mathbf{S}_{x,x}(k, l) = \mathbf{S}_{y,y}(k, l) = I(\omega_k)c(\tilde{\omega}_0)I(\omega_l)^*. \tag{35}$$

In [25], it is demonstrated that (35) is applicable for a nonlinear resistor in which band-to-band GR transitions occur. In this approach, the device is a homogeneously doped resistor so that the microscopic noise sources do not vary. When the microscopic noise sources are functions of the instantaneous bias, it is not known if it is possible to use an expression like (32) to describe the equivalent input current noise generator. In the literature, the modulated stationary noise model has been applied in general to low-frequency noise [5], [6], although it is not known if it is appropriate for all types of low-frequency noise.

Commercial circuit simulators, such as Agilent Advanced design system (ADS), treat low-frequency noise as being dependent on the dc component of the current flowing through the device [27]. However, such a model does not predict the presence of low-frequency noise around the USBs and LSBs under ac short-circuited conditions, as was observed for a linear resistor and a p^+-n junction [12]. In the next section, we present simulation results which compare (35) with a semiconductor noise simulation under periodic large-signal conditions.

IV. Simulation Results

A. Shot Noise

A silicon $n^+/p/n$ BJT was simulated in FLOODS with the dimensions and doping profile shown in Fig. 5. The 0.15-μm emitter contact is located at the upper-left corner and was modeled with a surface recombination velocity of $S_p = 10^5$ cm/s. The collector contact is along the bottom and the 0.15-μm base contact is located at the upper-right-hand side. The device had an emitter depth of 70 nm and a base width of 70 nm. The Klaassen mobility model [28] at 300 K was used for all simulations.

The diffusion noise for increasing dc bias on the base was simulated for $V_{CE} = 2.0$ V. The simulation results for base and collector shot noise versus V_{BE} are shown in Fig. 6. These results agreed well with the shot noise expressions of $S_{i_b} = 2qI_b$ and $S_{i_c} = 2qI_c$.

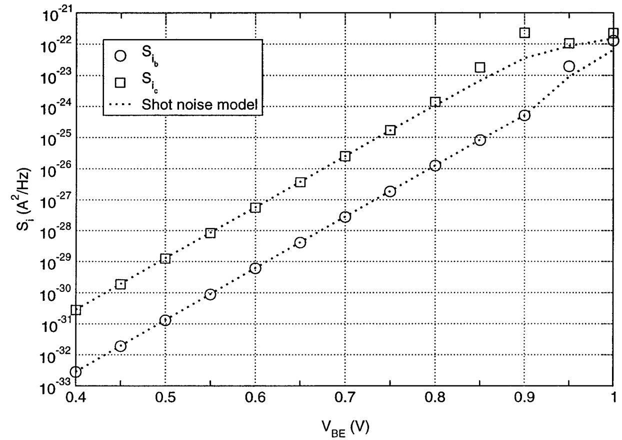

Fig. 6. Base and collector shot noise of the BJT.

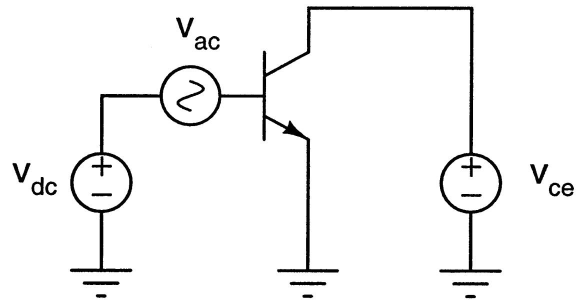

Fig. 7. Test circuit for the harmonic balance and noise simulation.

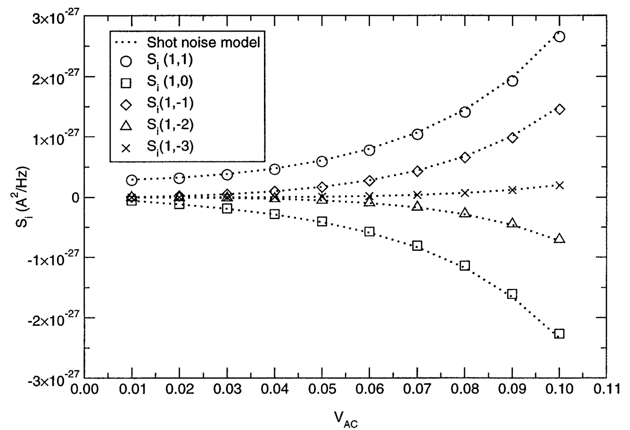

Fig. 8. Cross-spectral current densities for base shot noise for increasing ac bias. Symbols denote device simulation of (7) and dashed lines are calculated from (26).

For the HB simulation, the circuit shown in Fig. 7 was used with $v_{dc} = 0.7$ V, $v_{ce} = 2.0$ V and $v_{ac} = -V_{AC}\cos(2\pi 10^6 t)$ V. A noise simulation was performed for each sideband for increasing AC bias. The steady-state simulation was performed with five frequencies, including dc. This results in a conversion matrix relating nine sideband frequencies. Fig. 8 shows the cross-spectral current densities for the base current between the first USB and other sidebands denoted by $S_i(1, k)$, where

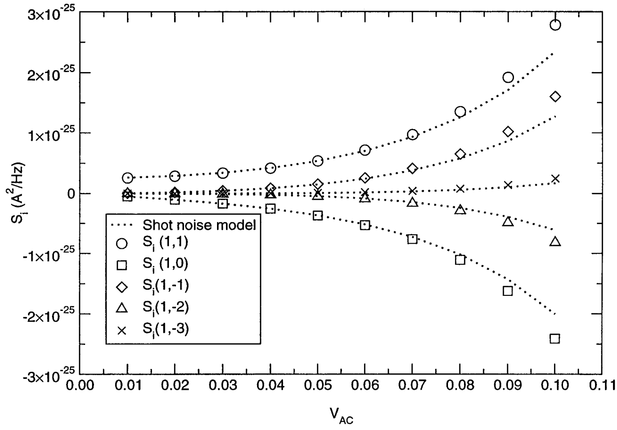

Fig. 9. Cross-spectral current densities for collector shot noise. Dotted lines use the model described by (26).

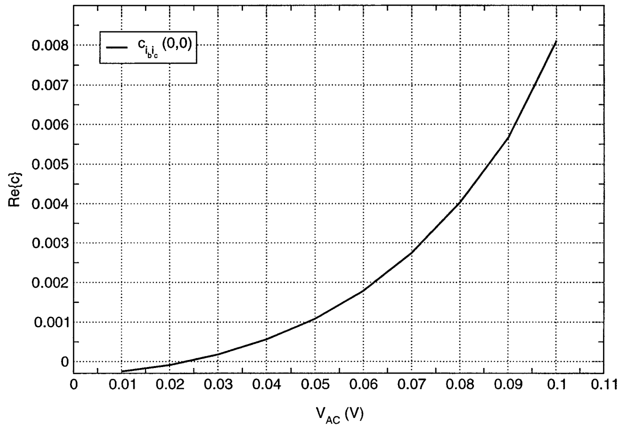

Fig. 10. Real part of the correlation between the base and collector shot noise at the BB for increasing ac bias. Imaginary part was negligible.

k denotes the sideband at frequency $\tilde{\omega}_k$. Excellent agreement was found between the simulated data and the NCM entry for shot noise given by (26).

Collector shot noise for increasing ac bias is shown in Fig. 9. The simulation begins to deviate from (26) for higher ac bias. This corresponds to the deviation between the simulation and analytical shot-noise model for the dc results shown in Fig. 6 and is attributed to high-level injection effects.

Fig. 10 shows the correlation between the base and collector shot noise at $\tilde{\omega}_0$ which was calculated as

$$c = \frac{S_{i_b,\,i_c}(0,\,0)}{\sqrt{S_{i_b}(0,\,0)S_{i_c}(0,\,0)}}. \tag{36}$$

This indicates that the equivalent current noise generators for the base and collector can be treated independently, even under large-signal ac conditions. Similar results were found when the cross correlation between the base and collector noise was evaluated at each sideband frequency.

B. GR Noise

The same BJT device was simulated with an electron capture coefficient of $c_n = 10^{-12}$ cm^3/s and an energy level of $E_C - E_T = 0.31$ eV. Similar trap parameters were reported for

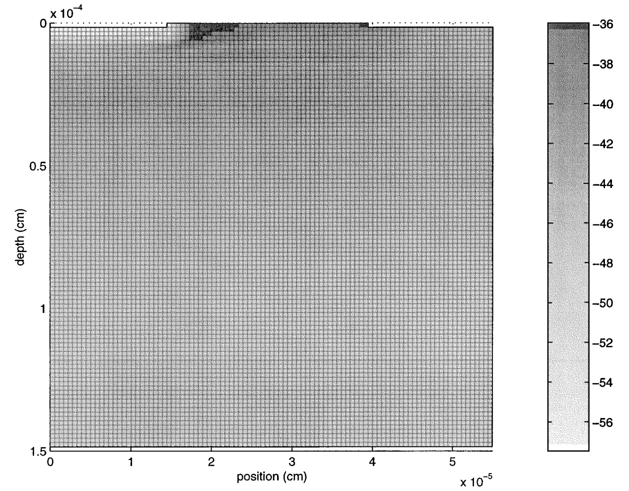

Fig. 11. Relative noise contributions of GR noise to the base current noise. Greyscale units are $\log_{10} \partial S_{i_b}/\partial r$.

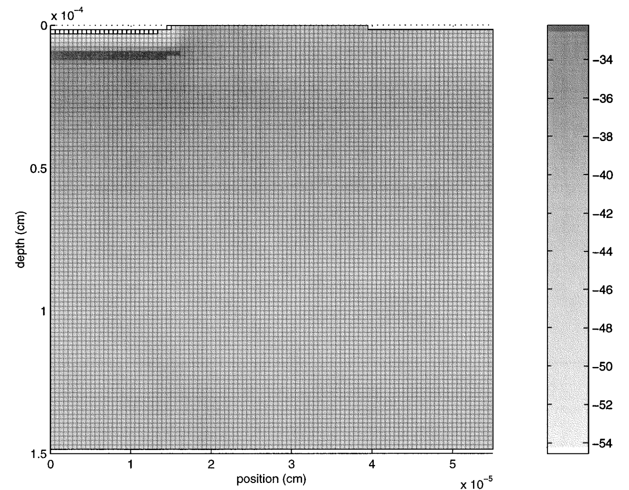

Fig. 12. Relative noise contributions of GR noise to the collector current noise. Greyscale units are $\log_{10} \partial S_{i_c}/\partial r$.

a polysilicon-emitter BJT in the literature [29] with the traps ascribed to the emitter region at or near the polysilicon–monosilicon interface. A constant trap density of $N_t = 1/\text{cm}^3$ was simulated for the device in order to find the relative contributions of the device regions. The distributed contributions to the short-circuit base current noise and collector current noise for $V_{BE} = 0.7$ V are shown in Figs. 11 and 12, respectively. For this trap energy level, the dominant noise contribution to the base noise is between the base and the emitter near the surface. A possible source of traps for this region would be the interface between the silicon and the oxide spacer between the base and emitter contacts [26].

Noise was then simulated for donor-like traps at a depth of 0 μm (see Fig. 5) between the base and emitter contact with $N_t^D = 8 \times 10^9/\text{cm}^2$.[1] Figs. 13 and 14 show both the GR and shot noise versus current at the base and collector, respectively. Fig. 15 shows the electron quasi-Fermi level for $V_{BE} = 0.7$ V at the surface of the device. It shows that near this bias condition, the electron quasi-Fermi-level is close to the trap-level

[1]The surface density is a volume density distributed over 1.5 nm at the surface.

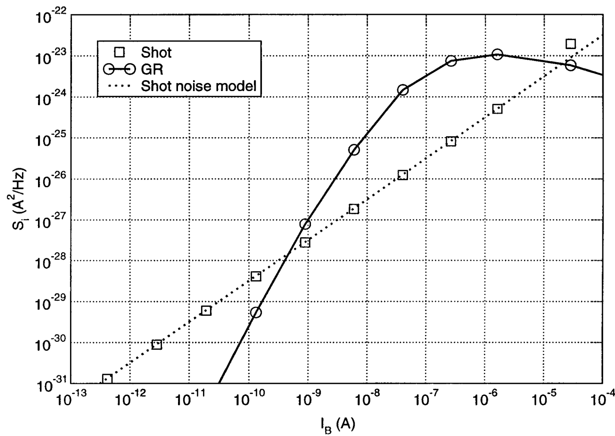

Fig. 13. Shot and GR current noise at the base versus I_B for dc bias conditions. Symbols denote device simulation and the dotted line is calculated from $S_i = 2qI_B$.

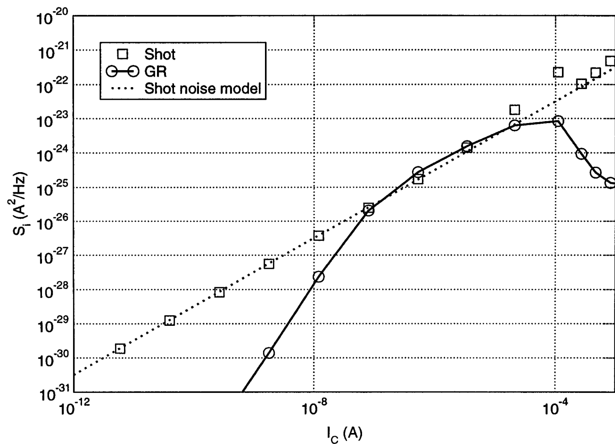

Fig. 14. Shot and GR current noise at the collector versus I_C.

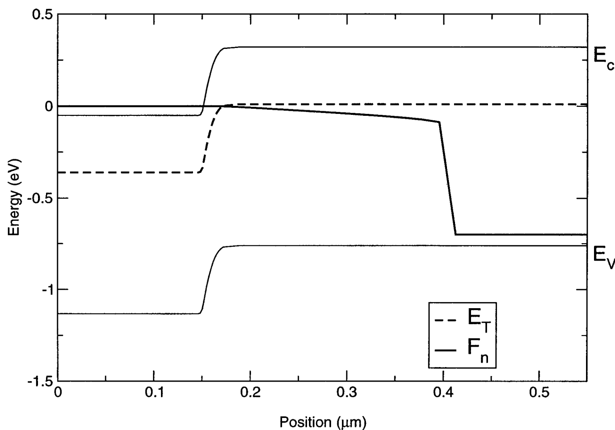

Fig. 15. Electron quasi-Fermi level F_n and the trap energy level E_T at the surface for $V_{BE} = 0.7$ V. Active traps for noise are where E_T and F_n intersect.

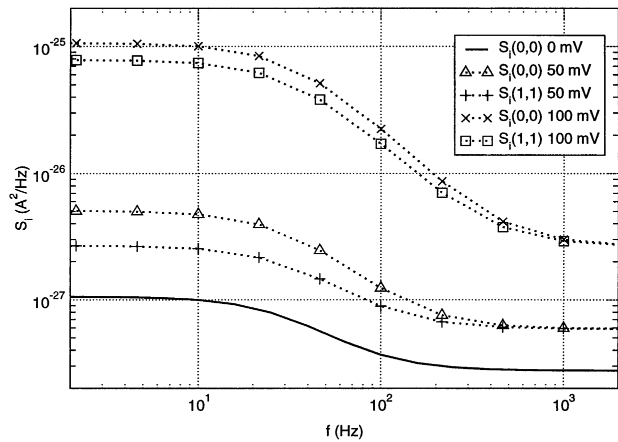

Fig. 16. Upper sideband and baseband noise spectra of the base terminal current for 2 large-signal ac bias values. Low-frequency plateau is due to the trap-assisted GR noise. High-frequency plateau is the diffusion noise floor.

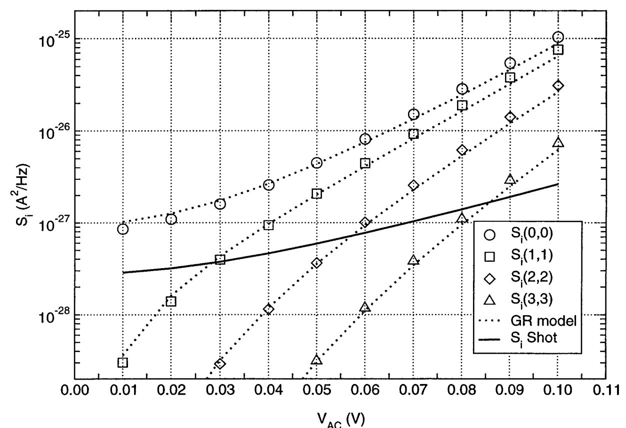

Fig. 17. Device simulation of upper sideband GR noise plateaus using (6) versus large-signal ac bias compared with circuit simulation using (35). Simulations were performed to the base terminal current. Symbols denote device simulation and dotted lines denote circuit simulation.

over the entire interface between the contacts. At lower biases a quadratic dependence of noise spectral density on dc current is observed and is attributed to trapping noise in the space charge region of the device. As bias is increased, the space charge region narrows, and the position where the quasi-Fermi level for electrons crosses the trap level moves into the quasi-neutral region and the quadratic current dependence is lost. At much higher biases, a high-level injection of electrons causes the location of this crossing to move toward the base contact so the area of active traps is reduced and the noise rolls off.

Using the same bias conditions as in Section IV-A the noise in the base terminal current was simulated versus frequency for increasing ac bias. In Fig. 16, the USB and BB spectra are shown for an ac bias of 0, 50, and 100 mV. The low-frequency plateau is the GR noise component while the high-frequency plateau is the diffusion noise floor. It is apparent that the corner frequency $f_c = 40$ Hz is invariant to the ac bias. The USB plateaus versus ac bias are shown in Fig. 17. The BB level was fit to the NCM model of (35) and (33) with $C = 1.21 \times 10^{-9}$/Hz and using the dc component of the base current for increasing ac bias. Using this value of C and the harmonics of the base current, the resistor GR noise model was applied to each of the sidebands in Fig. 17 and good agreement was found between device simulation of (6) and the circuit model. Fig. 18 shows the base current CSD between the first USB and several other sidebands. Again, good agreement was found between device simulation and the circuit model.

Fig. 19 shows the simulated GR spectrum at the BB and USB at 50 mV ac bias. In addition, the magnitude of their CSD is

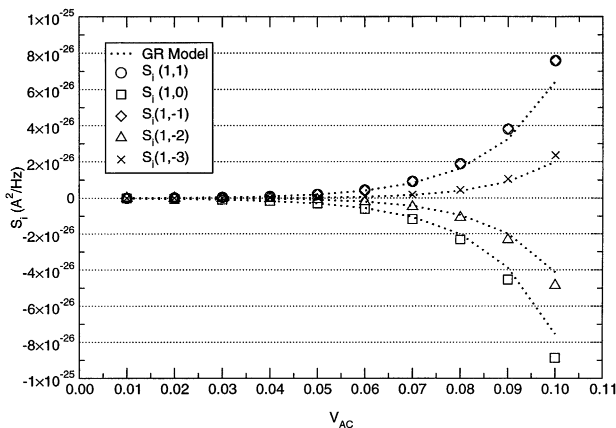

Fig. 18. Device simulation of the cross-spectral density of the low-frequency GR plateaus to the first USB for increasing ac bias. Simulations were performed to the base terminal current. Symbols denote device simulation and dotted lines denote circuit simulation.

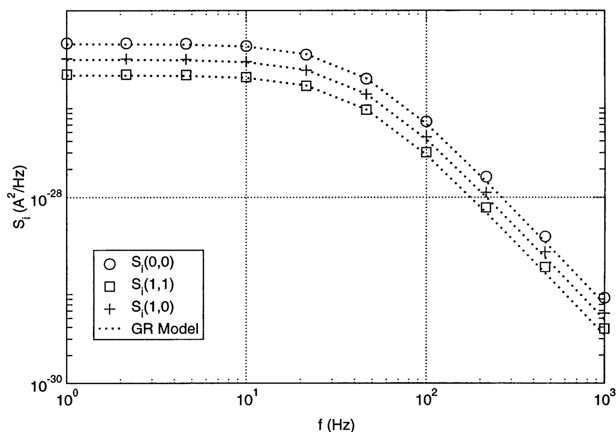

Fig. 19. Device simulation of the GR noise spectrum at the baseband and upper sideband and their cross-spectral density. Simulated NCM using (33) is shown with dotted lines.

shown. Using the value of C and $\tau = 1/2\pi f_c$ in (33), good agreement was found between the microscopic GR model and the equivalent NCM model.

The GR noise shown in the simulations had a near quadratic dependence on current. The good agreement for the stationary fluctuation model derived as (32) and the simulations was surprising since the the noise producing trapped carrier density was a function of instantaneous bias and the current dependence shown in Fig. 13 did not have an exact exponent of 2. This variation is attributed to the spatial position of active traps versus bias. In [11], the authors model low-frequency GR and flicker noise as being microscopically stationary and consider equivalent current density noise sources. They speculate that since the bias is varying at a frequency much larger than the corner frequency of the noise, that the trap is not able to respond.

In Fig. 16, the low-frequency GR noise rapidly increases about two orders of magnitude over the diffusion noise floor as the ac bias increases. This demonstrates that the effects of GR noise which is not considered significant in dc measurement or simulation may become important in mixer circuit or phase noise as the ac bias is increased. This effect depends on the circuit boundary conditions that the device is presented with.

In the literature, (32) is typically used for cyclostationary noise analysis in noise simulators without experimental or theoretical verification. The simulations presented in this paper provide evidence that such a model is applicable to low-frequency noise due to trap-assisted GR noise. The trap-assisted GR model could not be applied to the case of cyclostationary effects in MOSFET's, where the trapping occurs into the oxide [30]. It is, therefore, not known if this model could always be applied when the spectral density of the noise has a quadratic dependence on current such as for mobility fluctuations [21] or tunneling fluctuations through the mono/polysilicon interface of BJTs [26]. The simulation results in this section do provide evidence that the cyclostationary noise model can be applied to BJTs when traps are near the Si–SiO_2 interface at the device surface.

V. Conclusion

This paper presents the 2-D semiconductor device simulations of diffusion and GR noise under periodic large-signal conditions. In addition, our work indicates that a semiconductor device simulator can be used to justify and develop circuit noise modeling approaches. We also show that low-frequency noise due to trap-assisted GR fluctuations can be modeled using the modulated stationary noise model for the purposes of circuit simulation.

Acknowledgment

The authors would like to thank the reviewers for their careful reading of this manuscript and helpful suggestions. The authors would also like to thank F.-C. Hou and D. Martin for their participation in the development of noise simulation capabilities in FLOODS.

References

[1] F. Bonani, S. D. Donati, G. Ghione, and M. Pirola, "A TCAD approach to the physics-based modeling of frequency conversion and noise in semiconductor devices under large-signal forced operation," *IEEE Trans. Electron Devices*, vol. 48, pp. 966–977, May 2001.
[2] K. Mayaram, D. C. Lee, S. Moinian, D. A. Rich, and J. Roychowdhury, "Computer-aided circuit analysis tools for RFIC simulation: Algorithms, features, and limitations," *IEEE Trans. Circ. Syst. II*, vol. 47, pp. 274–286, Apr. 2000.
[3] C. Dragone, "Analysis of thermal and shot noise in pumped resistive diodes," *Bell Syst. Tech. J.*, vol. 47, pp. 1883–1902, 1968.
[4] D. N. Held and A. R. Kerr, "Conversion loss and noise of microwave and millimeter-wave mixers: Part 1—Theory," *IEEE Trans. Microwave Theory Tech.*, vol. MTT-26, pp. 49–54, Feb. 1978.
[5] A. Demir and A. Sangiovanni-Vincentelli, *Analysis and Simulation of Noise in Nonlinear Electronic Circuits and Systems*. Boston, MA: Kluwer, 1998.
[6] J. S. Roychowdhury, D. Long, and P. Feldmann, "Cyclostationary noise analysis of large RF circuits with multitone excitations," *IEEE J. Solid-State Circuits*, vol. 33, pp. 324–336, Mar. 1998.
[7] A. van der Ziel, "Unified presentation of $1/f$ noise in electronic devices: Fundamental $1/f$ noise sources," *Proc. IEEE*, vol. 76, pp. 233–258, Mar. 1988.
[8] W. Shockley, J. A. Copeland, and R. P. James, "The impedance field method of noise calculation in active semiconductor devices," in *Quantum Theory of Atoms, Molecules, and the Solid-State*, P.-O. Lowdin, Ed. New York: Academic, 1966, pp. 537–563.
[9] K. M. van Vliet, "Noise and admittance of the generation-recombination current involving SRH centers in the space-charge region of junction devices," *IEEE Trans. Electron Devices*, vol. ED-23, pp. 1236–1246, Nov. 1976.

[10] F. Bonani, G. Ghione, M. R. Pinto, and R. K. Smith, "An efficient approach to noise analysis through multidimensional physics-based models," *IEEE Trans. Electron Devices*, vol. 45, pp. 261–269, Jan. 1998.

[11] A. Cappy, F. Danneville, G. Dambrine, and B. Tamen, "Noise analysis in devices under nonlinear operation," *Solid-State Electron.*, vol. 43, pp. 21–26, 1999.

[12] J. E. Sanchez, G. Bosman, and M. E. Law, "Device simulation of generation-recombination noise under periodic large-signal conditions," in *IEDM Tech. Dig.*, 2001, pp. 477–480.

[13] M. Liang and M. E. Law, "Influence of lattice self-heating and hot-carrier transport on device performance," *IEEE Trans. Electron Devices*, vol. 41, pp. 2391–2398, Dec. 1994.

[14] ——, "An object-oriented approach to device simulation—FLOODS," *IEEE Trans. Computer-Aided Design*, vol. 13, pp. 1235–1240, Oct. 1994.

[15] B. A. Kramer, "Frequency conversion analysis of noise in heterojunction bipolar transistor oscillators including periodically modulated noise sources," Ph.D. dissertation, Iowa State Univ., Ames, IA, 1993.

[16] K. S. Kundert, J. K. White, and A. Sangiovanni-Vincentelli, *Steady-State Methods for Simulating Analog and Microwave Circuits*. Norwell, MA: Kluwer, 1990.

[17] B. Troyanovsky, Z. Yu, and R. W. Dutton, "Physics-based simulation of nonlinear distortion in semiconductor devices using the harmonic balance method," *Comput. Methods Appl. Mech. Eng.*, vol. 181, no. 4, pp. 467–482, Jan. 2000.

[18] Y. Hu and K. Mayaram, "Periodic steady-state analysis for coupled device and circuit simulation," in *Proc. IEEE SISPAD*, 2000, pp. 90–93.

[19] S. S. Li, *Semiconductor Physical Electronics*. New York: Plenum, 1993.

[20] W. J. McCalla, *Fundamentals of Computer-Aided Simulation*. Boston, MA: Kluwer, 1987.

[21] F. N. Hooge, "$1/f$ noise sources," *IEEE Trans. Electron Devices*, vol. 41, pp. 1926–1935, Nov. 1994.

[22] S. A. Maas, *Microwave Mixers*, 2nd ed. Norwood, MA: Artech House, 1993.

[23] A. van der Ziel, *Noise in Solid State Devices and Circuits*. New York: Wiley, 1986.

[24] J. H. J. Lorteije and A. M. H. Hoppenbrouwers, "Amplitude modulation by $1/f$ noise in resistors results in $1/\Delta f$ noise," *Philips Res. Rep.*, vol. 26, no. 1, pp. 29–39, 1971.

[25] F. Bonani, S. D. Guerrieri, and G. Ghione, "Noise source modeling for cyclostationary noise analysis in large-signal device operation," *IEEE Trans. Electron Devices*, vol. 49, pp. 1640–1647, Sept. 2002.

[26] M. J. Deen, J. Ilowski, and P. Yang, "Low frequency noise in polysilicon-emitter bipolar junction transistors," *J. Appl. Phys.*, vol. 77, no. 12, pp. 6278–6288, June 1995.

[27] *Agilent Advanced Design System*. Palo Alto, CA: Agilent Technologies, 2000.

[28] D. B. M. Klaassen, "A unified mobility model for device simulation—I. Model equations and concentration dependence," *Solid-State Electron.*, vol. 35, no. 7, pp. 953–959, June 1992.

[29] M. Sandén, O. Marinov, M. Deen, and M. Ostling, "A new model for the low-frequency noise and the noise level variation in polysilicon emitter BJTs," *IEEE Trans. Electron Devices*, vol. 49, pp. 514–520, Mar. 2002.

[30] E. A. M. Klumperink, S. L. J. Gierkink, A. P. van der Wel, and B. Nauta, "Reducing MOSFET $1/f$ noise and power consumption by switched biasing," *IEEE J. Solid-State Circuits*, pp. 994–1001, 2000.

Juan E. Sanchez (S'92–M'03) received the B.S.E.E. degree in 1995 from the University of South Florida, Tampa, and the M.S. and Ph.D. degrees from the University of Florida, Gainesville, in 1997 and 2002, respectively, both in electrical and computer engineering.

His graduate research concerned measurement and semiconductor device simulation of noise under periodic large-signal conditions. He is now with Synopsys, Inc., Mountain View, CA, where he is a TCAD R&D Engineer. His research interests include RF-related issues in semiconductor device simulation.

Dr. Sanchez is a member of the IEEE Electron Device Society.

Gijs Bosman (SM'01) received the B.S., M.S., and Ph.D. degrees in physics from the University of Utrecht, Utrecht, The Netherlands in 1971, 1976, and 1981, respectively.

In 1981, he joined the Department of Electrical and Computer Engineering, University of Florida, Gainesville, where he is currently a Professor and Associate Chair. His research interests include the electrical noise and charge transport properties of semiconductor devices and circuits. He has published more than 100 refereed journal and conference papers on these topics. He is an Editor of *Fluctuations and Noise Letters*.

Dr. Bosman was the General Chair and host of the 16th International Conference on Noise in Physical Systems and $1/f$ Fluctuations, held in Gainesville, FL, in the fall of 2001. He serves on the International Advisory Committee on Noise and Fluctuations. He is a Member of the American and Dutch Physical societies. In addition to the College of Engineering Teacher of the Year Award for 1998–1999, he has received several university and departmental awards for teaching and research.

Mark E. Law (F'98) received the B.S.Cpr.E. degree from Iowa State University, Ames, in 1982, and the M.S.E.E. degree and the Ph.D. degree from Stanford University, Stanford, CA, in 1982 and 1988, respectively.

He is a Professor of electrical and computer engineering at the University of Florida (UF), Gainesville. He worked at Hewlett Packard from 1982 to 1985 and joined the faculty at Florida in 1988. He is currently Co-Director of the Software and Analysis of Advanced Materials Processing (SWAMP) center at UF. His current research interests include integrated circuit process modeling and characterization. As a graduate student, he coauthored SUPREM-IV, and his research group at (UF) developed the Florida Object Oriented Process Simulator (FLOOPS). His research has focused on the modeling of point defects and dopant diffusion in silicon. He has written over 100 papers in the area of process and device modeling.

Dr. Law was named a National Science Foundation Presidential Faculty Fellow in 1992, Outstanding Young Alumni of Iowa State in 1994, College of Engineering Teacher of the Year in 1996–1997, and a UF Research Fellow in 1998. The FLOOPS development effort won the 1993 Semiconductor Research Corporation (SRC) Technical Excellence Award. He was Editor-in-Chief of the IEEE JOURNAL ON TECHNOLOGY COMPUTER-AIDED DESIGN from 1992 to 2002 and has served as an Editor of IEEE TRANSACTIONS ON SEMICONDUCTOR MANUFACTURING. He chaired the 1997 Simulation of Semiconductor Process and Devices Meeting, the 1999 Silicon Front-End Processing Symposium of the Materials Research Society, and chaired the 2000 International Electron Devices Meeting. He has served on technical committees for several other conferences.